InP-Based Near Infrared/Extended-Short Wave Infrared Dual-Band Photodetector

Zongheng Xie, Zhuo Deng, Xinbo Zou, *Member, IEEE*, and Baile Chen, *Member, IEEE*

***Abstract*— In this paper, InP based near infrared (NIR) /extended-short wave infrared (eSWIR) dual-band photodetector with $In_{0.53}$ $Ga_{0.47}$ As and $In_{0.53}$ $Ga_{0.47}$ As/$GaAs_{0.5}$ $Sb_{0.5}$ type-II superlattice (T2SL) back-to-back *n-i-p/p-i-n* structures is demonstrated. Monolithic growth of NIR/eSWIR dual-band photodetector on InP substrate enjoys the benefit of the lattice matched property of InP/InGaAs/GaAsSb material system. Low optical crosstalk (below -10 dB) between the two sub-detector is achieved for wavelength range out of 1690-1750 nm. At room temperature, the device exhibits a dark current density of 1.26×10^{-5} A/cm^2 for $In_{0.53}$ $Ga_{0.47}$ As sub-detector under -0.1 V bias and 3.78×10^{-2} A/cm^2 for $In_{0.53}$ $Ga_{0.47}$ As/$GaAs_{0.5}$ $Sb_{0.5}$ sub-detector under -1 V bias. The corresponding responsivity and specific detectivity are 0.57 A/W and 2.63×10^{11} cm· Hz$^{1/2}$/W at 1640 nm for NIR sub-detector and 0.22 A/W and 1.96×10^9 cm· Hz$^{1/2}$/W at 2 μm for eSWIR sub-detector, respectively. The characterization results show the potential for monolithically growing dual-band SWIR photodetector on InP substrate with low dark current density for SWIR applications.**

***Index Terms*— Dual-band, NIR/eSWIR photodetector, $In_{0.53}$ $Ga_{0.47}$ As PIN, $In_{0.53}$ $Ga_{0.47}$ As/$GaAs_{0.5}$ $Sb_{0.5}$ T2SL.**

I. Introduction

DUAL-BAND photodetectors have attracted long-term interests due to their potential applications in targets tracking, medical treatment and environmental monitoring [1]. Compared with the traditional single band photodetectors, dual/multiband infrared photodetectors can provide improved target identification and signal contrast of the chemical signatures [2]. So far, short wavelength infrared (SWIR)/ mid wavelength infrared (MWIR) photodetectors [3] and MWIR/long wavelength infrared (LWIR) photodetectors [4] based on InAs/GaSb or InAs/InAsSb type-II superlattices (T2SL) have been demonstrated.

Manuscript received April 15, 2020; revised July 2, 2020; accepted July 9, 2020. Date of publication July 13, 2020; date of current version July 21, 2020. This work was supported in part by the National Key Research and Development Program of China under Grant 2019YFB2203400, in part by the National Natural Science Foundation of China under Grant 61975121, in part by the Shanghai Sailing Program under Grant 17YF1429300, and in part by ShanghaiTech University under Grant F-0203-16-002. *(Corresponding author: Baile Chen.)*

Zongheng Xie is with the School of Information Science and Technology, ShanghaiTech University, Shanghai 201210, China, also with the Shanghai Institute of Microsystem and Information Technology, Chinese Academy of Sciences, Shanghai 200050, China, and also with the University of Chinese Academy of Sciences, Beijing 100049, China.

Zhuo Deng, Xinbo Zou, and Baile Chen are with the School of Information Science and Technology, ShanghaiTech University, Shanghai 201210, China (e-mail: chenbl@shanghaitech.edu.cn).

Color versions of one or more of the figures in this letter are available online at http://ieeexplore.ieee.org.

Digital Object Identifier 10.1109/LPT.2020.3008853

The SWIR spectral range emerged as very useful for several applications including enhanced imaging, security, remote sensing, light detection and ranging (LIDAR) and food inspection. There are very few dual-band photodetectors reported with both bands in the SWIR range. Campbell et al reported the dual-band InGaAsP photodetector in near infrared band [5]. Hamamatsu sells near infrared (NIR, 750-1700 nm) /extended short wavelength infrared (eSWIR, 1700-2500 nm) dual-band photodetector based on the InGaAs/InP material systems [6]. This two-color detector uses two InGaAs photodetectors with different In composition on InP substrate to detect the NIR band and eSWIR band. However, for eSWIR detection, InGaAs is not lattice matched to InP substrate, and the metamorphic growth could generate defects in the active region, which causes higher dark current and degrade the performance of the devices [7]. Moreover, for dual-band application, the package process also requires two chips with different In composition to be optically aligned, which is cumbersome and not compatible to focal plane array process.

$In_{0.53}Ga_{0.47}As/GaAs_{0.5}Sb_{0.5}$ T2SL has attracted significant attention for excellent performance in the SWIR band due to its lattice matching to InP substrate [8]–[17]. The bandgap of these T2SL can be tuned by changing the thickness and composition while remaining lattice matching or strain balance conditions [13], [18]. Based on the stability and robustness of the mature III–V compound technology on InP, the feasibility of T2SL covering the SWIR band have been reported.

In this study, we report the first dual-band detector based on $In_{0.53}Ga_{0.47}As$ bulk material and $In_{0.53}Ga_{0.47}As/GaAs_{0.5}Sb_{0.5}$ T2SL directly monolithically grown on InP substrate. The device can cover the NIR band from 1.0 to 1.7 μm and the eSWIR band from 1.7 to 2.7 μm. The device operating in NIR band shows a responsivity of 0.57 A/W and specific detectivity of 2.63×10^{11} cm· Hz$^{1/2}$/W at 1640 nm under -0.1 V bias. While operated in eSWIR band, the detector has responsivity of 0.22 A/W and specific detectivity of 1.96×10^9 cm· Hz$^{1/2}$/W at 2 μm under -1 V bias. The optical crosstalk between the two operation regions is below -10 dB, outside the wavelength range from 1690 to 1750 nm.

II. Experimental Details

The schematic structure of the dual-band detector grown on lattice matching InP substrate by solid source molecular beam epitaxy (MBE) is shown in Fig. 1 (a). The dual-band detector consists of two back-to-back *n-i-p/p-i-n* sub-detectors. The first sub-detector is for eSWIR detection based

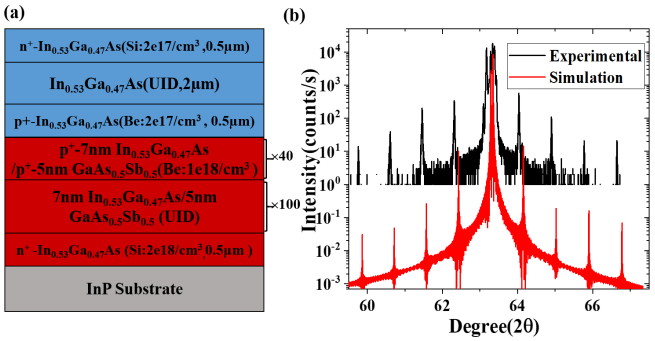

Fig. 1. (a) Schematic diagram of the dual-band photodetector; (b) High-resolution X-Ray diffraction pattern of the structure and simulation result. The black curve is the experimental result and the red curve is the simulation result.

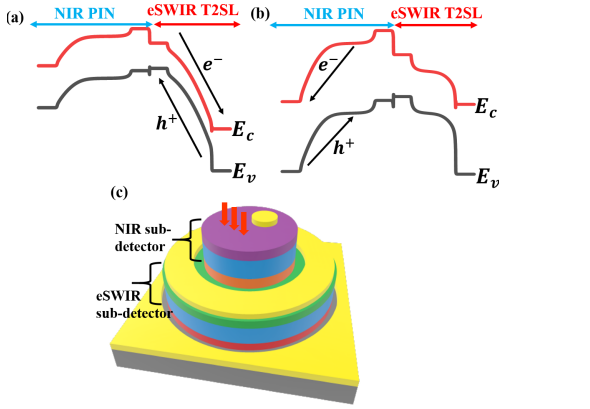

Fig. 2. (a) Band diagram of the device when eSWIR sub-detector is under -1V bias; (b) Band diagram of the device when NIR sub-detector is under -0.1V bias; (c) The device structure after fabrication.

on the $In_{0.53}Ga_{0.47}As/GaAs_{0.5}Sb_{0.5}$ T2SL for normal incidence detection. The eSWIR sub-detector consists of 0.5 μm n-doped $In_{0.53}Ga_{0.47}As$ layer, 100 pairs of unintentionally doped (UID) 7 nm $In_{0.53}Ga_{0.47}As$/ 5 nm $GaAs_{0.5}Sb_{0.5}$T2SL and p-doped 40 pairs of 7 nm $In_{0.53}Ga_{0.47}As$/ 5 nm $GaAs_{0.5}Sb_{0.5}$ T2SL. The NIR sub-detector is based on InGaAs n-i-p structure with 2 μm thickness of InGaAs i-region. To avoid the NIR light to be absorbed by the eSWIR sub-detector, which causes significant crosstalk, the eSWIR device is grown under the NIR sub-detector for front-illumination, in which case the InGaAs n-i-p also acts as NIR filter layer for eSWIR operation.

After material growth, the crystal quality of the wafer was studied by high-resolution X-ray diffraction (HRXRD), as shown in Fig.1 (b). The appearance of various satellite peaks indicates high crystal quality of the T2SL. The simulated XRD rocking curve of the detector structure is also shown in Fig.1 (b). It is clear that the peak positions are very close to that of the experimental curve. Period thickness d of the $In_{0.53}Ga_{0.47}As/GaAs_{0.5}Sb_{0.5}$ T2SL can be calculated by [19]:

$$d = \frac{\lambda}{2\Delta\theta cos\theta} \tag{1}$$

where λ =0.15406 nm is the wavelength of X-ray source,θ is the location of the main peak and $\Delta\theta$ is the interval between main and diffraction peaks. The calculated result shows that the thickness of one period of $In_{0.53}Ga_{0.47}As/GaAs_{0.5}Sb_{0.5}$ T2SL is 11.96 nm, which is very close to the designed thickness (12 nm).

After the material quality characterization, the wafer was processed into isolated double-mesa devices by standard UV photolithography as shown in Fig.2 (c). The top mesa has a diameter of 180 μm and the bottom mesa has a diameter of 340 μm. The double mesa structure was wet etched with the same H_3PO_4:H_2O_2:H_2O solution (1:1:10) and the etch of top mesa was stopped at p^+ InGaAs layer. Metal contacts of Ti/Pt/Au were deposited by e-beam evaporation and lift-off technique. No anti-reflection (AR) coating was applied in the device. The band diagrams of each sub-detector under working bias were simulated by Silvaco software and shown in Fig.2 (a) and (b).

III. Results and Discussions

The dark current-bias characteristics of the two sub-detectors were measured independently by semiconductor parameter analyzer (Keysight B1500A) in cryogenic probe station from 160 to 300 K. When the dark current of InGaAs sub-detector was tested, the bottom InGaAs/GaAsSb sub-detector was floating and vice versa when testing the InGaAs/GaAsSb sub-detector. The dark current-voltage curves of a 180 μm diameter $In_{0.53}Ga_{0.47}As$ NIR sub-detector at different temperature are shown in Fig. 3 (a). Noted that the noisy data at low temperature (160 K and 190 K) are due to the measurement limit of the analyzer. The dark current is 3.22×10^{-9}A at 300 K under -0.1 V, which corresponds to a dark current density of 1.26×10^{-5} A/cm^2. Fig.3 (b) shows the corresponding Arrhenius plot of the temperature dependent dark current. The activating energy (E_{a1}) is about 504 meV at high temperature region (220-300 K), suggesting the domination of generation-recombination (G-R) current. The dark current-voltage characteristics of the eSWIR $In_{0.53}Ga_{0.47}As/GaAs_{0.5}Sb_{0.5}$ T2SL sub-detector are shown in Fig. 3(c). At 300 K, the dark current is 3.43×10^{-5} A under -1 V bias corresponding to the dark current density of 3.78×10^{-2} A/cm^2. This value is slightly higher than that of the previously reported InGaAs/GaAsSb p-i-n photodiodes [20] and In-rich InGaAs photodiodes [21], [22] under similar bias condition, but lower than that of GaSb based single band or dual-band photodiodes [23], [24]. The Arrhenius plot under -1 V shown in Fig.3 (d) indicates an activation energy of around 241 meV at high temperature range (E_{a2}), which is about half the bandgap of 7 nm $In_{0.53}Ga_{0.47}As$/5 nm $GaAs_{0.5}Sb_{0.5}$T2SL at high temperature. This indicates the dark current is also dominated by the G-R current. We also tested the dark current of devices with diameters from 70 to 500 μm. The dark current scales linearly with device area other than perimeter, suggesting that the dark current is mainly composed of bulk rather than surface component.

After electrical measurements, optical characterization was also carried out for both sub-detectors. The devices were cleaved and wire-bonded with a TO header. The external quantum efficiencies (EQE) of the devices were calibrated

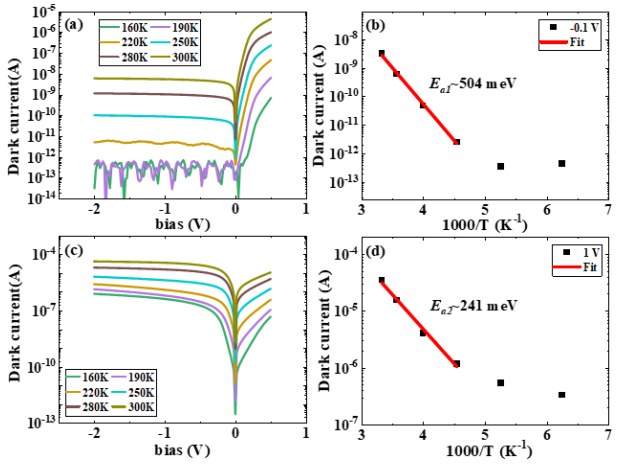

Fig. 3. (a) Dark current-voltage characteristic of the NIR sub-detector from 160K-300 K; (b) Arrhenius plot and the linear fits of the NIR sub-detector dark current under -0.1 V bias; (c) Dark current-voltage characteristic of the eSWIR sub-detector from 160 K-300 K; (d) Arrhenius plot and the linear fits of the eSWIR sub-detector dark current under -1 V bias.

by a Thorlabs standard Ge detector (part No. FDG03-CAL) and In-rich InGaAs detector (part No. PDA10DT-EC). The light from a halogen source passed through a monochromator and then the monochromatic light was modulated by a chopper at 180 Hz. The modulated light was collimated by a parabolic mirror and then fully concentrated on the surface of the device. When the EQE of one sub-detector was tested, the other sub-detector was shorted to minimize the crosstalk between two sub-detectors. Based on the EQE measurement, it is found that the EQE of NIR sub-detector saturates around -0.1 V, while that of eSWIR sub-detector saturates around -1 V, which could be due to potential higher background doping (extracted from C-V measurements) in *i*-InGaAs/GaAsSb T2SL of eSWIR sub-detector than that in *i*-InGaAs layer of NIR sub-detector (1.0×10^{16} cm^{-3} vs 2.2×10^{14} cm^{-3}). The corresponding room temperature EQE of the NIR sub-detector under -0.1 V and the eSWIR sub-detector under -1 V are shown in Fig. 4 (a). At 1550 nm, the above $In_{0.53}Ga_{0.47}As$ sub-detector exhibits an EQE of 47 % and at 2 μm, the T2SL sub-detector has EQE of 13.5 %. Compared with the commercial InGaAs photodetector, the QE of InGaAs sub-detector is relatively lower, which is attributed to low carrier collection efficiency in the 0.5 μm *n*-type InGaAs contact layer.

To investigate the optical isolation characteristics of the dual-band structure, we define the optical crosstalk C as:

$$C = -20log_{10}\frac{\max(QE_{NIR}, QE_{eSWIR})}{\min(QE_{NIR}, QE_{eSWIR})} dB \qquad (2)$$

where QE_{NIR} and QE_{eSWIR} is the quantum efficiency of NIR sub-detector and eSWIR sub-detector, respectively. Eq.2 is defined based on the change in ratio between photocurrent of the two sub-detector [25]. The relative crosstalk magnitude and a -10 dB line are plotted as a function of wavelength in Fig. 4 (b). As shown in figure, the crosstalk has a peak at 1720 nm and quickly drops to -10 dB outside of 1690-1750 nm range. It should be noted that the

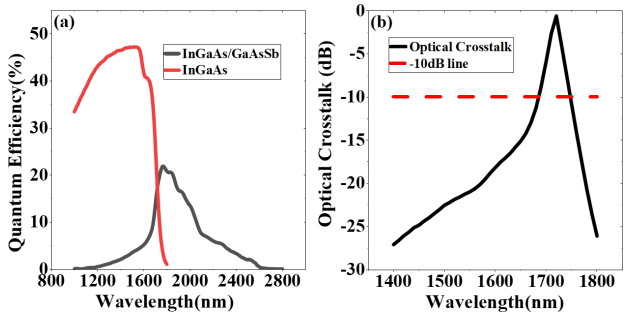

Fig. 4. (a) EQE measured for $In_{0.53}Ga_{0.47}As$ NIR sub-detector (under -0.1 V) and $In_{0.53}Ga_{0.47}As/GaAs_{0.5}Sb_{0.5}$ T2SL eSWIR sub-detector (under -1 V); (b) Relative inter-detector optical crosstalk as a function of wavelength.

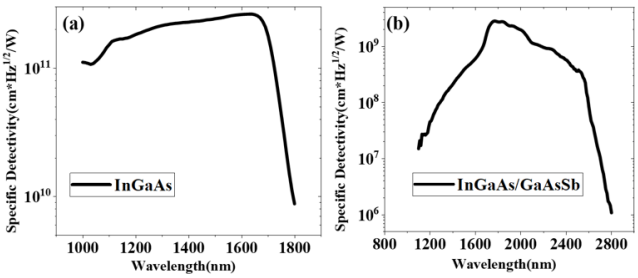

Fig. 5. Room temperature specific detectivity measured for (a) $In_{0.53}Ga_{0.47}As$ NIR sub-detector and (b) $In_{0.53}Ga_{0.47}As/GaAs_{0.5}Sb_{0.5}$ T2SL eSWIR sub-detector.

optical crosstalk is determined by the transparency of InGaAs sub-detector (i.e., thickness) and the carrier collection in the eSWIR detector, which can be further optimized in future epitaxial design.

Finally, the specific detectivity D$*$ was calculated by [26]:

$$D^* = \frac{R}{\sqrt{\frac{4k_BT}{R_0A} + 2qJ_d}} \qquad (3)$$

where R is the responsivity,k_B is Boltzmann's constant, T is the test temperature, R_0A is the differential-resistance area product under zero bias, q is the electron charge and J_d is the dark current density under bias. Fig. 5 depicts the calculated $D*$ of the NIR and eSWIR sub-detector. The NIR sub-detector has a $D*$ of 2.63×10^{11} cm· $Hz^{1/2}$/W at 1640 nm and the eSWIR sub-detector has a $D*$ of 1.96×10^9 cm· $Hz^{1/2}$/W at 2 μm. Compared with the commercial InGaAs based dual-band photodetector [6], which has a typical value of 5×10^{12} cm· $Hz^{1/2}$/W at NIR range and 7×10^{10} cm· $Hz^{1/2}$/W at eSWIR range, the current NIR/eSWIR dual-band detector based on T2SL is about an order of magnitude lower in $D*$. Thus, in order to achieve higher device performance comparable with the more mature InGaAs based dual-band structure, while still enjoying the advantages of T2SL, additional engineering on the current structure should be focused on reduction of defect density in the sub-detector, such as the interface defects between InGaAs/GaAsSb, as well as optimization of the epitaxial design.

IV. Conclusion

In conclusion, optically-aligned *n-i-p/p-i-n* back-to-back $In_{0.53}Ga_{0.47}As$ NIR and $In_{0.53}Ga_{0.47}As/GaAs_{0.5}Sb_{0.5}$ T2SL eSWIR dual-band photodetector has been demonstrated in this work. The room temperature dark current density of NIR sub-detector is 1.26×10^{-5} A/cm^2 under -0.1V bias and the dark current density of eSWIR sub-detector is 3.78×10^{-2}A/cm^2 under -1 V bias. Meanwhile, the responsivity of the two sub-detectors is 0.57 A/W at 1640 nm and 0.22 A/W at 2μm, respectively, and the corresponding detectivity reaches 2.63×10^{11} cm$\cdot$ Hz$^{1/2}$/W and 1.96×10^{9} cm$\cdot$ Hz$^{1/2}$/W. Excellent electrical isolation of the two sub-detectors has also been shown, with the optical crosstalk drops below -10 dB outside of 1690-1750 nm range. To improve the performance of this dual-band photodetector, some future works are proposed such as using transparent *n*-InP layer as the top contact layer, incorporating thicker absorber, and optimizing the growth of T2SL. In addition, adding an electron barrier layer between the two sub-detectors can further improve optical crosstalk. Last but not the least, structure with the eSWIR sub-detector on top of NIR sub-detector could also be potentially used for dual-color imaging arrays.

References

[1] A. K. Sood *et al.*, "Design and development of two-dimensional strained layer superlattice (SLS) detector arrays for IR applications," in *Two-Dimensional Materials for Photodetector*, J. Trdine, Ed. Rijeka, Croatia: InTechOpen, 2018.

[2] A. Haddadi, R. Chevallier, G. Chen, A. M. Hoang, and M. Razeghi, "Bias-selectable dual-band mid-/long-wavelength infrared photodetectors based on InAs/InAs$_{1-x}$Sb$_x$ type-II superlattices," *Appl. Phys. Lett.*, vol. 106, no. 1, Jan. 2015, Art. no. 011104, doi: 10.1063/1.4905565.

[3] A. M. Hoang, G. Chen, A. Haddadi, and M. Razeghi, "Demonstration of high performance bias-selectable dual-band short-/mid-wavelength infrared photodetectors based on type-II InAs/GaSb/AlSb superlattices," *Appl. Phys. Lett.*, vol. 102, no. 1, Jan. 2013, Art. no. 011108.

[4] A. Haddadi, A. Dehzangi, R. Chevallier, S. Adhikary, and M. Razeghi, "Bias–selectable nBn dual–band long–/very long–wavelength infrared photodetectors based on InAs/InAs$_{1-x}$Sb$_x$/AlAs$_{1-x}$Sb$_x$ type–II superlattices," *Sci. Rep.*, vol. 7, no. 1, Dec. 2017, Art. no. 011104.

[5] J. Campbell, A. Dentai, T. Lee, and C. Burrus, "Improved two-wavelength demultiplexing InGaAsP photodetector," *IEEE J. Quantum Electron.*, vol. 16, no. 6, pp. 601–603, Jun. 1980.

[6] Hamamatsu. *Two-Color Detector K12729-010K*. Accessed: 2020 [Online]. Available: https://www.hamamatsu.com/jp/en/product/type/K12729-010K/index.html

[7] C. Li, Y. Zhang, K. Wang, Y. Gu, H. Li, and Y. Li, "Distinction investigation of InGaAs photodetectors cutoff at 2.9 μm," *Infr. Phys. Technol.*, vol. 53, no. 3, pp. 173–176, May 2010.

[8] W. Chen, B. Chen, J. Yuan, A. Holmes, and P. Fay, "Bulk and interfacial deep levels observed in $In_{0.53}Ga_{0.47}As/GaAs_{0.5}Sb_{0.5}$ multiple quantum well photodiode," *Appl. Phys. Lett.*, vol. 101, no. 5, Jul. 2012, Art. no. 052107.

[9] B. Chen and L. H. Archie, "Carrier dynamics in InP-based PIN photodiodes with InGaAs/GaAsSb type-II quantum wells," *J. Phys. D, Appl. Phys.*, vol. 46, no. 31, Aug. 2013, Art. no. 315103.

[10] B. Chen, J. Yuan, and A. Holmes, Jr., "Dark current modeling of InP based SWIR and MWIR InGaAs/GaAsSb type-II MQW photodiodes," *Opt. Quantum Electron.*, vol. 45, no. 3, pp. 271–277, 2012.

[11] B. Chen, W. Y. Jiang, J. Yuan, A. L. Holmes, and B. M. Onat, "Demonstration of a room-temperature InP-based photodetector operating beyond 3 μm," *IEEE Photon. Technol. Lett.*, vol. 23, no. 4, pp. 218–220, Feb. 15, 2011.

[12] Y. Chen and B. Chen, "Design of InP-based high-speed photodiode for 2-μm wavelength application," *IEEE J. Quantum Electron.*, vol. 55, no. 1, pp. 1–8, Feb. 2019.

[13] B. Chen, W. Y. Jiang, and A. L. Holmes, "Design of strain compensated InGaAs/GaAsSb type-II quantum well structures for mid-infrared photodiodes," *Opt. Quantum Electron.*, vol. 44, nos. 3–5, pp. 103–109, Jun. 2012.

[14] Y. Chen, Z. Xie, J. Huang, Z. Deng, and B. Chen, "High-speed unitraveling carrier photodiode for 2 μm wavelength application," *Optica*, vol. 6, no. 7, pp. 884–889, 2019.

[15] B. Chen and A. L. Holmes, "InP-based short-wave infrared and midwave infrared photodiodes using a novel type-II strain-compensated quantum well absorption region," *Opt. Lett.*, vol. 38, no. 15, pp. 2750–2753, 2013.

[16] H. Inada *et al.*, "Low dark current SWIR photodiode with InGaAs/GaAsSb type II quantum wells grown on InP substrate," in *Proc. IEEE Int. Conf. Indium Phosph. Rel. Mater.*, May 2009, pp. 149–152.

[17] R. Sidhu, N. Duan, J. C. Campbell, and A. L. Holmes, "A long-wavelength photodiode on InP using lattice-matched GaInAs-GaAsSb type-II quantum wells," *IEEE Photon. Technol. Lett.*, vol. 17, no. 12, pp. 2715–2717, Dec. 2005.

[18] J. F. Klem, S. R. Kurtz, and A. Datye, "Growth and properties of GaAsSb/InGaAs superlattices on InP," *J. Cryst. Growth*, vol. 111, nos. 1–4, pp. 628–632, 1991.

[19] S. A. Speakman, "Estimating crystallite size using XRD," *MIT Center Mater. Sci. Eng.*, pp. 3–8, 2014.

[20] B. Chen, W. Jiang, J. Yuan, A. L. Holmes, and B. M. Onat, "SWIR/MWIR InP-based p-i-n photodiodes with InGaAs/GaAsSb type-II quantum wells," *IEEE J. Quantum Electron.*, vol. 47, no. 9, pp. 1244–1250, Sep. 2011.

[21] Y. Arslan, F. Oguz, and C. Besikci, "Extended wavelength SWIR InGaAs focal plane array: Characteristics and limitations," *Infr. Phys. Technol.*, vol. 70, pp. 134–137, May 2015.

[22] Y. Liu *et al.*, "Surface leakage behaviors of 2.6 μm $In_{0.83}Ga_{0.17}As$ photodetectors as a function of mesa etching depth," *IEEE J. Quantum Electron.*, vol. 56, no. 2, pp. 1–6, Apr. 2020.

[23] T. D. Nguyen, J. O. Kim, Y. H. Kim, E. T. Kim, Q. L. Nguyen, and S. J. Lee, "Dual-color short-wavelength infrared photodetector based on InGaAsSb/GaSb heterostructure," *AIP Adv.*, vol. 8, no. 2, Feb. 2018, Art. no. 025015.

[24] J.-M. Wun, Y.-W. Wang, Y.-H. Chen, J. E. Bowers, and J.-W. Shi, "GaSb-based p-i-n photodiodes with partially depleted absorbers for high-speed and high-power performance at 2.5-μm wavelength," *IEEE Trans. Electron Devices*, vol. 63, no. 7, pp. 2796–2801, Jul. 2016.

[25] K. Swaminathan, T. J. Grassman, L.-M. Yang, Q. Gu, M. J. Mills, and S. A. Ringel, "Optically-aligned visible/near-infrared dual-band photodetector materials and devices on GaAs using metamorphic epitaxy," *J. Appl. Phys.*, vol. 110, no. 6, Sep. 2011, Art. no. 063109.

[26] Z. Deng *et al.*, "Demonstration of Si based InAs/GaSb type-II superlattice p-i-n photodetector," *Infr. Phys. Technol.*, vol. 101, pp. 133–137, Sep. 2019.